Reflection and transmission characteristics of Lamb waves at an adhesive lap joint of plates

Naoki Mori[a] and Takayuki Kusaka
Department of Mechanical Engineering, Ritsumeikan University, 1-1-1 Noji-higashi, Kusatsu, Shiga 525-8577, Japan

(Received 13 February 2019; revised 1 May 2019; accepted 4 May 2019; published online 28 May 2019)

The reflection and transmission characteristics of Lamb waves at an adhesive single lap joint of plates are examined theoretically by the hybrid finite element method. The adhesive joint is modeled by a linear spring-type interface, which is characterized by normal and tangential stiffnesses. For the incidence of the lowest-order antisymmetric (A0) Lamb mode in a low frequency range, it is shown that the reflection and transmission coefficients of the A0 mode take local maxima and minima at multiple frequencies. This behavior results from the interference of waves originating from the lowest-order antisymmetric guided wave mode in the overlap region. The peak frequencies of the transmission coefficient increase monotonically with increasing tangential stiffness, but are almost invariant with the normal stiffness of the adhesive joint. Furthermore, time-domain numerical simulation using the finite element method is carried out to discuss the theoretical results. As a result, for the A0 mode incidence, the reflection and transmission waveforms of the A0 mode from the lap joint are found to show long-oscillation tails. The spectral analysis for the obtained waveforms shows that these tails are necessary to identify the frequencies at which the reflection and transmission coefficients take local maxima and minima.
 https://doi.org/10.1121/1.5109098

[MCR] Pages: 3075–3085

I. INTRODUCTION

Adhesive bonding gains importance in many industrial fields, such as aircraft and automobiles, due to its advantage for lighter structures and multi-material design compared to other joining techniques. As the adhesive bonding becomes widespread, the necessity of the nondestructive evaluation (NDE) grows for adhesive joints of different structures. Ultrasonic waves play a major role in the NDE of adhesive joints, enabling not only the detection of gross defects, such as voids and cracks, but also the quantitative evaluation of the cohesive properties.[1–3] Furthermore, the adhesive property, i.e., the property of adhesive interfaces, is also important to maintain the integrity of adhesive joints.[4–8] The interfacial adhesion is significantly affected by the surface treatment of adherends before bonding, which includes abrasion to control the surface roughness and alcohol cleaning to eliminate the surface contamination.

In the ultrasonic NDE of plate-like structures, elastic guided waves attract great attention due to relatively long propagation distances compared to bulk waves. In isotropic plates, two types of guided waves, i.e., shear-horizontal (SH) guided waves and Lamb waves, can mainly propagate.[9] The deformations of the SH guided waves are parallel to the plate surfaces and normal to the propagation direction, while the Lamb waves show deformations normal to those of the SH guided waves.

Numerous studies were carried out to examine the application of the guided waves to the NDE of adhesive joints.[7–23] For a single lap joint of plates, Lowe *et al.*[12] performed a finite element simulation of the Lamb wave transmission across a lap joint for the incidence of the lowest-order symmetric (S0) Lamb mode, showing the effect of the bond length and thickness on the transmission characteristics. Lanza di Scalea *et al.*[14] measured the transmission characteristics at a lap joint for the incidence of the lowest-order antisymmetric (A0) Lamb mode, which were shown to depend on the cohesive properties of the adhesive layer. It was revealed in previous studies that the length, thickness, and cohesive properties of the adhesive layer affect the Lamb wave transmission characteristics across a lap joint, but the effect of the adhesive interface on the Lamb wave transmission has not sufficiently been explored.[20] On the other hand, the transmission characteristics of SH guided waves for different adhesive interfacial conditions were shown by Castaings,[19] who modeled an adhesive joint as a thin viscoelastic layer with spring-type interfaces and estimated the tangential stiffness of the adherend-adhesive interfaces from the transmission waveform.

The aim of the present study is to examine the reflection and transmission characteristics of Lamb waves at a single lap joint of plates. In particular, the effect of the adhesive interface is taken into account in two-dimensional theoretical analysis using the hybrid finite element method (HFEM). Among various types of adhesively bonded joints, single lap joints with relatively thin adhesive layers are considered in this study.

This paper is structured as follows. In Sec. II, the theoretical model of a single lap joint of plates is explained. The adhesive joint is modeled as a spring-type interface, which is

[a]Electronic mail: nmori@fc.ritsumei.ac.jp

characterized by normal and tangential stiffnesses. The formulation of the HFEM in the frequency domain is also briefly described. In Sec. III, the reflection and transmission characteristics for the A0 mode incidence are shown and discussed by comparing to the results in a multi-reflection model. Furthermore, the peak frequencies of the A0 mode transmission coefficient are particularly examined. In Sec. IV, time-domain numerical simulation using the finite element method (FEM) is carried out. The results by the time-domain analysis are used to check the validity of the theoretical results and discuss the interpretation of the temporal waveforms.

II. NUMERICAL MODEL AND METHOD

A. Lap joint model

As shown in Fig. 1, in the x-y-z Cartesian coordinate system, two semi-infinite isotropic and linear elastic plates of thickness d overlap each other and are jointed in $|x| < L/2$, where L is the overlap length. The two adherends are under the plane-strain condition in the x-z plane. The wave propagation in the plates obeys the two-dimensional Navier equation in the frequency domain

$$\begin{aligned}
&\left(c_{\mathrm{L}}^2 - c_{\mathrm{T}}^2\right)\frac{\partial}{\partial x}\left(\frac{\partial u_x}{\partial x} + \frac{\partial u_z}{\partial z}\right) + c_{\mathrm{T}}^2\left(\frac{\partial^2}{\partial x^2} + \frac{\partial^2}{\partial z^2}\right)u_x = -\omega^2 u_x,\\
&\left(c_{\mathrm{L}}^2 - c_{\mathrm{T}}^2\right)\frac{\partial}{\partial z}\left(\frac{\partial u_x}{\partial x} + \frac{\partial u_z}{\partial z}\right) + c_{\mathrm{T}}^2\left(\frac{\partial^2}{\partial x^2} + \frac{\partial^2}{\partial z^2}\right)u_z = -\omega^2 u_z,
\end{aligned} \tag{1}$$

where ω is angular frequency, $u_x = u_x(x,z,\omega)$ and $u_z = u_z(x,z,\omega)$ are displacement components, and c_{L} and c_{T} are the velocities of longitudinal and transverse waves, respectively. On the plate surfaces, traction-free conditions are applied to the corresponding stress components. For the overlap region $|x| < L/2$, the adhesive joint is modeled as a linear spring-type interface[24–26]

$$\begin{aligned}
\sigma_z(x,0^+,\omega) &= \sigma_z(x,0^-,\omega)\\
&= K_{\mathrm{N}}\left[u_z(x,0^+,\omega) - u_z(x,0^-,\omega)\right],\\
\tau_{xz}(x,0^+,\omega) &= \tau_{xz}(x,0^-,\omega)\\
&= K_{\mathrm{T}}\left[u_x(x,0^+,\omega) - u_x(x,0^-,\omega)\right],
\end{aligned} \tag{2}$$

where $\sigma_z = \sigma_z(x,z,\omega)$ and $\tau_{xz} = \tau_{xz}(x,z,\omega)$ are stress components, and $z = 0^+$ ($z = 0^-$) represents the joint surface of the upper (lower) adherend. The parameters K_{N} and K_{T} denote normal and tangential stiffnesses of the adhesive joint, respectively, which were assumed to be uniform over the entire joint. The adhesive layer is replaced by equivalent distributed springs, and the effect of their thicknesses emerges in the normal and tangential stiffnesses of the joint.[4,25] This modeling is valid if the bond thickness h_A is sufficiently thin, i.e., $kh_A \ll 1$, where k is the wavenumber of a guided wave mode in the overlap region.[25–28] For a thicker adhesive layer, the overlap region should be modeled as a triple-layer structure. This topic is left for future studies.

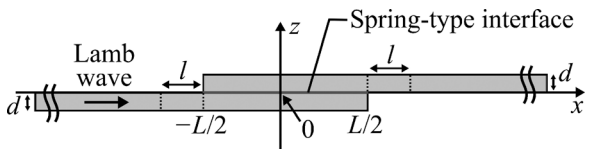

FIG. 1. Schematic of an adhesively bonded single lap joint of plates subjected to the Lamb wave incidence.

The incident frequency $f = \omega/(2\pi)$ is limited in $fd/c_{\mathrm{T}} < 0.25$, where only the S0 and A0 Lamb modes can propagate in the single plate regions. Other Lamb modes are non-propagating modes or evanescent modes in this frequency range. The A0 mode propagating in the positive x direction is incident to the lap joint, and the reflection and transmission behavior is analyzed by the HFEM. In this study, the material property of aluminum alloy ($c_{\mathrm{L}} = 6.4\,\mathrm{km/s}$, $c_{\mathrm{T}} = 3.17\,\mathrm{km/s}$, and mass density $\rho = 2.7 \times 10^3\,\mathrm{kg/m^3}$) was used for the modeling of the adherends.

B. HFEM

HFEM[31–34] was employed to examine the reflection and transmission characteristics at a lap joint subjected to the A0 mode incidence. As shown in Fig. 1, the bounded region $|x| < L/2 + l$, including the lap joint, was discretized by finite elements, where l denotes the length of single plate regions in the finite element model. The propagation behavior of the guided waves in this region was analyzed by frequency-domain FEM. In the semi-infinite single plate regions $|x| > L/2 + l$, the displacement fields $\mathbf{u} = (u_x \;\; u_z)^{\mathrm{T}}$ were expressed by the superposition of different Lamb modes in a single plate as

$$\begin{aligned}
\mathbf{u} = {}& \mathbf{U}_{+0}^{\mathrm{A}} \exp\left(\mathrm{i}k_{+0}^{\mathrm{A}}x\right)\\
&+ \sum_{n=0}^{\infty}\left[R_{\mathrm{A}n}\mathbf{U}_{-n}^{\mathrm{A}}\exp(\mathrm{i}k_{-n}^{\mathrm{A}}x) + R_{\mathrm{S}n}\mathbf{U}_{-n}^{\mathrm{S}}\exp(\mathrm{i}k_{-n}^{\mathrm{S}}x)\right],
\end{aligned} \tag{3}$$

in $x < -L/2 - l$ and

$$\mathbf{u} = \sum_{n=0}^{\infty}\left[T_{\mathrm{A}n}\mathbf{U}_{+n}^{\mathrm{A}}\exp(\mathrm{i}k_{+n}^{\mathrm{A}}x) + T_{\mathrm{S}n}\mathbf{U}_{+n}^{\mathrm{S}}\exp(\mathrm{i}k_{+n}^{\mathrm{S}}x)\right], \tag{4}$$

in $x > L/2 + l$, respectively, where $\mathrm{i} = \sqrt{-1}$, $\mathbf{U}_{+n}^{\beta}$ ($\mathbf{U}_{-n}^{\beta}$) is the displacement profile vector of the nth-order Lamb mode propagating or decaying in the positive (negative) x direction, the superscripts $\beta = \mathrm{S}$ and $\beta = \mathrm{A}$ represent the symmetric and antisymmetric modes, respectively, and k_{+n}^{β} and k_{-n}^{β} are the wavenumbers of the corresponding Lamb modes. The time-dependent term $\exp(-\mathrm{i}\omega t)$ is omitted from all terms in Eqs. (3) and (4), where t denotes time. The coefficients $R_{\beta n}$ and $T_{\beta n}$ are the reflection and transmission coefficients of each Lamb mode, respectively. By applying the continuity condition of the displacement and stress components at nodes along the boundaries $|x| = L/2 + l$, the reflection and transmission coefficients were obtained.

To confirm the validity of the numerical calculation, the case of the overlap length $L = d$ was first examined

according to Song *et al.*,[35] who imposed the continuity condition on the displacement and stress components at $z=0$. Their numerical analysis corresponds to the case of infinite normal and tangential stiffnesses (K_N, $K_T \to \infty$) in the present study. Accordingly K_N and K_T were set as sufficiently high values for comparison, $K_T d/\mu = 100$ and $K_T/K_N = 0.4$, where $\mu = \rho {c_T}^2$ is the shear modulus of the adherends. In this study, joint conditions are expressed by the normalized tangential stiffness $K_T d/\mu$ and the stiffness ratio K_T/K_N. The infinite series in Eqs. (3) and (4) were truncated at $n=7$, since only the finite number of Lamb modes can be considered in the numerical calculation. When the bounded area $|x| < L/2 + l$ was discretized by four-node square-shaped isoparametric elements of size length $d/10$, the length l was obtained as $l = 0.5d$ to keep the quantity based on the energy conservation[34]

$$\delta = \left| 1 - \frac{E_R + E_T}{E_I} \right|, \tag{5}$$

within 2.5%, where E_I, E_R, and E_T are the energy fluxes of the incident, reflected, and transmitted waves, respectively.

For the A0 mode incidence, the amplitude reflection and transmission coefficients of the A0 mode calculated by HFEM, $|R_{A0}|$ and $|T_{A0}|$, are shown as functions of the normalized frequency fd/c_T in Fig. 2(a). The obtained results are found to be in good agreement with the reflection and transmission coefficients given in Ref. 35. Furthermore, the S0 mode is generated by mode conversion due to the thickness variation at the joint edges $|x| = L/2$. The amplitude reflection and transmission coefficients of the S0 mode are shown in Fig. 2(b). The mode conversion characteristics reported in Ref. 35 are also well reproduced by HFEM. From these results, the validation of the numerical calculation by HFEM for sufficiently high joint stiffnesses is confirmed. In Secs. III and IV, the numerical parameters shown above are used, and relatively long single lap joints of length $L = 15d$ are considered. The reflection and transmission of Lamb waves at a lap joint are analyzed for different normal and tangential stiffnesses.

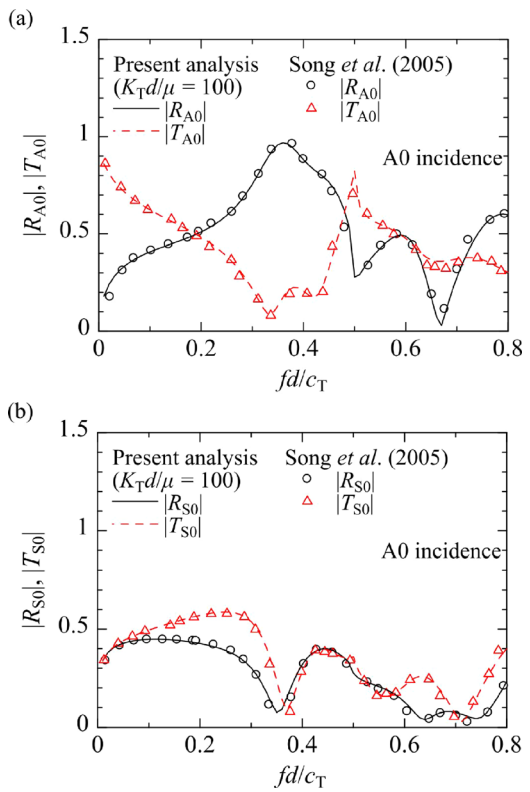

FIG. 2. (Color online) Comparison of the amplitude reflection and transmission coefficients of the (a) A0 and (b) S0 modes calculated by HFEM to the results in Ref. 35 for the A0 mode incidence.

III. RESULTS AND DISCUSSIONS

A. Reflection and transmission coefficients for the A0 mode incidence

For the A0 mode incidence, the reflection and transmission characteristics at a lap joint of length $L = 15d$ are analyzed by HFEM. The amplitude reflection and transmission coefficients of the A0 and S0 modes, $|R_{A0}|$, $|T_{A0}|$, $|R_{S0}|$, and $|T_{S0}|$, are shown as functions of the normalized frequency fd/c_T for different tangential stiffnesses $K_T d/\mu$ in Figs. 3(a)–3(d), respectively, where a stiffness ratio K_T/K_N is fixed as $K_T/K_N = 0.4$. It is reported in previous studies that the stiffness ratio K_T/K_N is roughly between 0.2 and 0.6.[4,21,25,26] In Figs. 3(a)–3(d), the expression $K_T d/\mu = \infty$ represents the results for infinite stiffnesses, at which the continuity condition is applied to both displacement and stress components at $z=0$ in the overlap region. Each coefficient in Figs. 3(a)–3(d) varies with frequency in a complicated manner and takes local maxima and minima at multiple frequencies. These local maximum and minimum frequencies, i.e., the locations of the local maxima and minima, respectively, depend on the tangential stiffness.

The effect of the stiffness ratio K_T/K_N on the reflection and transmission coefficients for the A0 mode incidence is examined. The amplitude reflection and transmission coefficients of the A0 and S0 modes are shown for different stiffness ratios at a fixed tangential stiffness $K_T d/\mu = 4$ in Figs. 4(a)–4(d). As a result, it is found that the stiffness ratio, i.e., the normal stiffness, does not significantly affect the reflection and transmission coefficients of the A0 and S0 modes for the A0 mode incidence. In particular, the local maximum and minimum frequencies of the reflection and transmission coefficients are shown to be almost invariant with the normal stiffness. This interesting feature is reported for the first time in the present study and is further investigated in Sec. III C.

Since some adhesives show non-negligible viscoelastic properties, the effect of the damping on the reflection and transmission coefficients is investigated. When the adhesive has viscoelastic properties, the normal and tangential stiffnesses of Eq. (2) are expressed as complex numbers,[29] i.e., $K_N = K_{N0} - i\alpha_N$ and $K_T = K_{T0} - i\alpha_T$. Based on the viscoelastic moduli of an adhesive shown in Ref. 30, the imaginary parts of K_N and K_T were set as $\alpha_N = 0.1K_{N0}$ and $\alpha_T = 0.1K_{T0}$ here, respectively. The obtained reflection and transmission coefficients of the A0 mode for the A0 mode incidence are shown in Figs. 5(a)–5(d) for two different tangential stiffnesses at $K_T/K_N = 0.4$. These results are compared to the

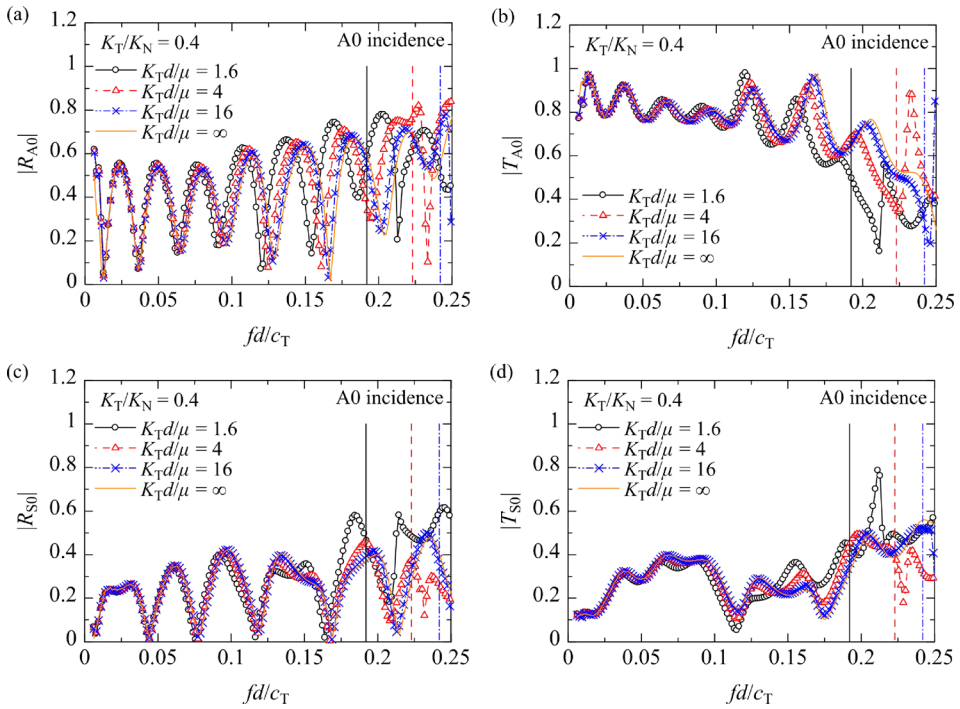

FIG. 3. (Color online) Variation of the amplitude (a) reflection and (b) transmission coefficients of the A0 mode, and the amplitude (c) reflection and (d) transmission coefficients of the S0 mode for the A0 mode incidence with the normalized incident frequency, for different tangential stiffnesses K_Td/μ at a stiffness ratio $K_T/K_N = 0.4$. For reference, a vertical line shows the cutoff frequency of the DA1 mode at each tangential stiffness, which is introduced in Sec. III B.

ones without the attenuation ($\alpha_N = \alpha_T = 0$). When the tangential stiffness is relatively high, i.e., $K_{T0}d/\mu = 16$, the effect of the attenuation factors α_N and α_T on the reflection and transmission coefficients is insignificant, as shown in Figs. 5(a) and 5(b). On the other hand, at $K_{T0}d/\mu = 1.6$, the peaks and valleys of the reflection and transmission coefficients in Figs. 5(c) and 5(d) become dull due to the attenuation as the normalized frequency increases. However, as long as the viscoelastic properties of a common adhesive are assumed, the local maximum and minimum frequencies of the reflection and transmission coefficients are almost invariant in this frequency range. In Secs. III B, III C, and IV, the numerical analysis is further carried out with the attenuation factors set as $\alpha_N = \alpha_T = 0$.

B. Comparison to the multi-reflection model

To discuss the reflection and transmission characteristics at a lap joint, particularly the local maxima and minima of the reflection and transmission coefficients, a multi-reflection model that combines three configurations is employed, as schematically shown in Figs. 6(a)–6(c). This model is used to examine the roles of guided wave modes in the overlap region for the reflection and transmission

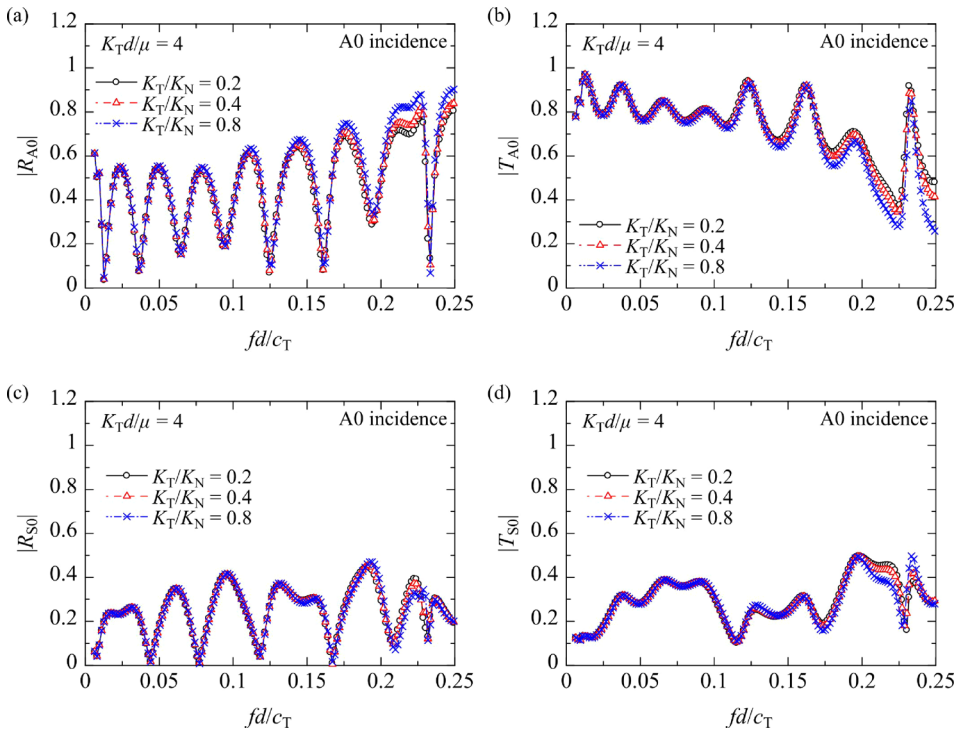

FIG. 4. (Color online) Variation of the amplitude (a) reflection and (b) transmission coefficients of the A0 mode, and the amplitude (c) reflection and (d) transmission coefficients of the S0 mode for the A0 mode incidence with the normalized incident frequency for different stiffness ratios K_T/K_N at a tangential stiffness $K_Td/\mu = 4$.

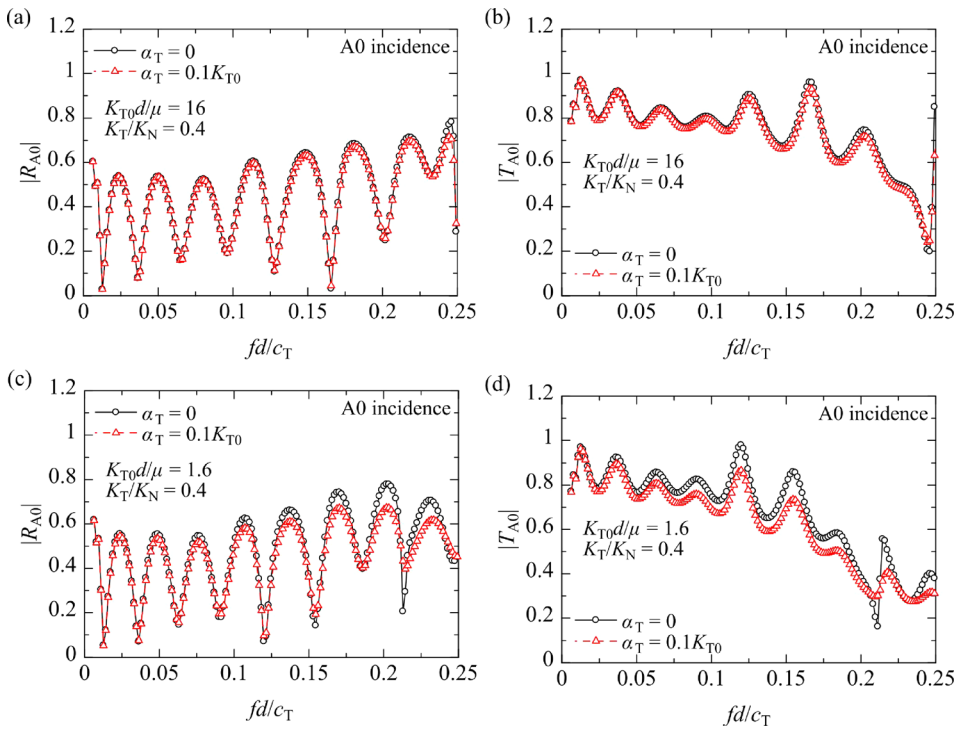

FIG. 5. (Color online) Comparison of the reflection and transmission coefficients at $\alpha_T = 0$ (without attenuation) and $\alpha_T = 0.1K_{T0}$ (with attenuation) for the A0 mode incidence at a stiffness ratio $K_T/K_N = 0.4$: the amplitude (a) reflection and (b) transmission coefficients of the A0 mode at $K_{T0}d/\mu = 16$, and the amplitude (c) reflection and (d) transmission coefficients of the A0 mode at $K_{T0}d/\mu = 1.6$.

coefficients of the A0 mode across the lap joint. A similar model was used in the discussion of the guided wave reflection and transmission behavior at a lap joint.[12,35] In Figs. 6(a)–6(c), only the reflection and transmission at a joint edge are considered. In the overlap region, i.e., a double-layer plate coupled with a spring-type interface, guided wave modes that are similar to Lamb waves propagate. When the thicknesses of the upper and lower adherends are equal, the guided wave modes in the overlap region can be classified into symmetric and antisymmetric modes.[36] Mezil *et al.*[36] showed that the dispersion relations of the symmetric and antisymmetric modes depend only on the normal and tangential stiffnesses, respectively, due to the symmetry of their deformations. The wavenumber-frequency relations of the symmetric and antisymmetric modes are shown in Figs. 7(a) and 7(b) for different normal and tangential stiffnesses, respectively. The vertical axes in Figs. 7(a) and 7(b) represent

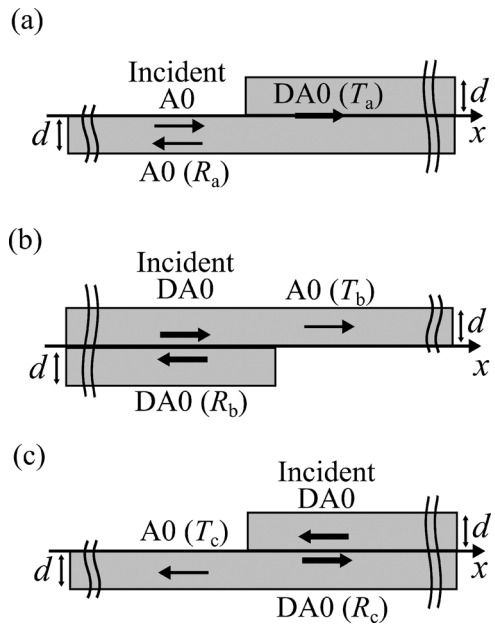

FIG. 6. Multi-reflection model, which combines the following three configurations: (a) the A0 mode incidence to the left edge of the lap joint, (b) the DA0 mode incidence to the right edge of the lap joint, and (c) the DA0 mode incidence to the left edge of the lap joint.

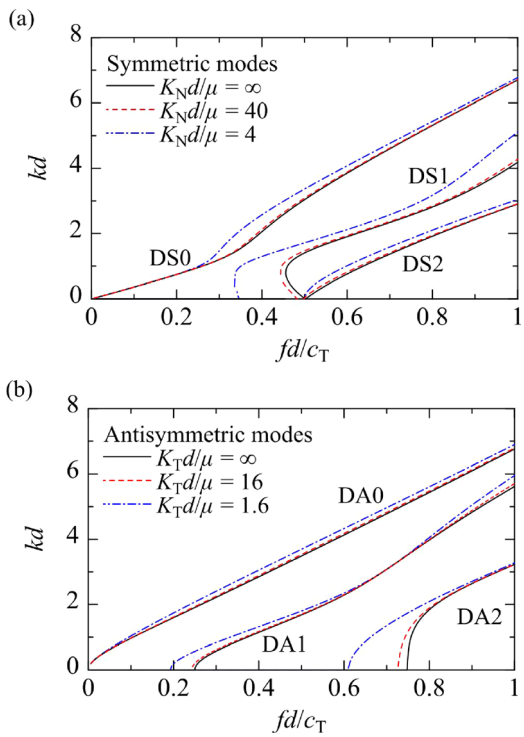

FIG. 7. (Color online) Wavenumber-frequency relations of the (a) symmetric and (b) antisymmetric guided wave modes in the overlap region of thickness $2d$, i.e., a double-layer plate with a spring-type interface, for different normal and tangential stiffnesses, respectively.

the products of the wavenumber k and the adherend thickness d. As the normal and tangential stiffnesses become high, the dispersion relations approach the results for a single-layer plate with double thickness $2d$. In a sufficiently low frequency range, only the lowest-order symmetric (DS0) and antisymmetric (DA0) guided wave modes can propagate in the double-layer plates. The cutoff frequency of the DA1 mode is located in $fd/c_T < 0.25$ and depends on the tangential stiffness.

In the numerical model of Fig. 6(a), the A0 mode is incident from the lower plate to the left edge of the lap joint, and the reflection and transmission characteristics at the edge are analyzed by HFEM. Similarly to the formulation of the HFEM for the lap joint model in Sec. II B, the bounded region of length $2l$, including the joint edge, was discretized by finite elements, and the wave fields outside the region were expressed as the superpositions of different modes. Namely, the displacement fields in the left and right semi-infinite regions were given by the superpositions of Lamb wave modes in the single-layer plate and guided wave modes in the double-layer plate, respectively. The reflection coefficient of the A0 mode in the single-layer plate and the transmission coefficient of the DA0 mode in the double-layer plate are denoted as R_a and T_a, respectively. In the numerical model of Fig. 6(b), the DA0 mode propagating in the positive x direction is incident to the right edge of the joint, while the DA0 mode propagating in the negative x direction is incident to the left edge of the joint in Fig. 6(c). The reflection coefficient of the DA0 mode and the transmission coefficient of the A0 mode are expressed as R_b and T_b for Fig. 6(b), and R_c and T_c for Fig. 6(c), respectively. From these three numerical models, the reflected and transmitted A0 modes at a lap joint of finite length L are obtained as the superpositions of the waves generated by multiple reflection between the joint edges. When only the DA0 mode is considered as a propagating mode in the overlap region, the reflection and transmission coefficients of the A0 mode in the multi-reflection model, $R_{A0,MR}$ and $T_{A0,MR}$, are given in a similar manner to Refs. 37 and 38 by infinite series

$$\begin{aligned} R_{A0,MR} &= R_a + T_a R_b \exp\left(2ik_0^{DA}L\right) T_c \\ &\quad \times \sum_{n=0}^{\infty} \left[R_c R_b \exp\left(2ik_0^{DA}L\right)\right]^n \\ &= R_a + \frac{T_a R_b T_c \exp\left(2ik_0^{DA}L\right)}{1 - R_c R_b \exp\left(2ik_0^{DA}L\right)}, \\ T_{A0,MR} &= T_a \exp\left(ik_0^{DA}L\right) T_b \sum_{n=0}^{\infty} \left[R_b R_c \exp\left(2ik_0^{DA}L\right)\right]^n \\ &= \frac{T_a \exp\left(ik_0^{DA}L\right) T_b}{1 - R_b R_c \exp\left(2ik_0^{DA}L\right)}, \end{aligned} \tag{6}$$

respectively, where k_0^{DA} is the wavenumber of the DA0 mode.

The amplitude reflection and transmission coefficients of the A0 mode calculated from Eq. (6) are compared to the results for the lap joint model in Figs. 8(a) and 8(b) for two tangential stiffnesses. The reflection and transmission coefficients obtained from the multi-reflection model show local maxima and minima, which are in good agreement with the results for the lap joint model in a low frequency range even if the propagation of the DS0 mode in the overlap region is neglected. Namely, the local maxima and minima of the A0 mode reflection and transmission coefficients result from the interferences of the A0 Lamb waves, which originate from the interaction of the DA0 mode with the joint edges. As the incident frequency becomes high, however, the A0 mode reflection and transmission coefficients based on the multi-reflection model begin to deviate from the results of the lap joint model. This deviation appears because in the multi-reflection model only the DA0 mode is considered as the propagating mode in the overlap region. By incorporating the propagation of other modes such as the DS0 mode, the results for the multi-reflection model could agree better with the lap joint model in a higher frequency range, but further investigation is not performed in this study.

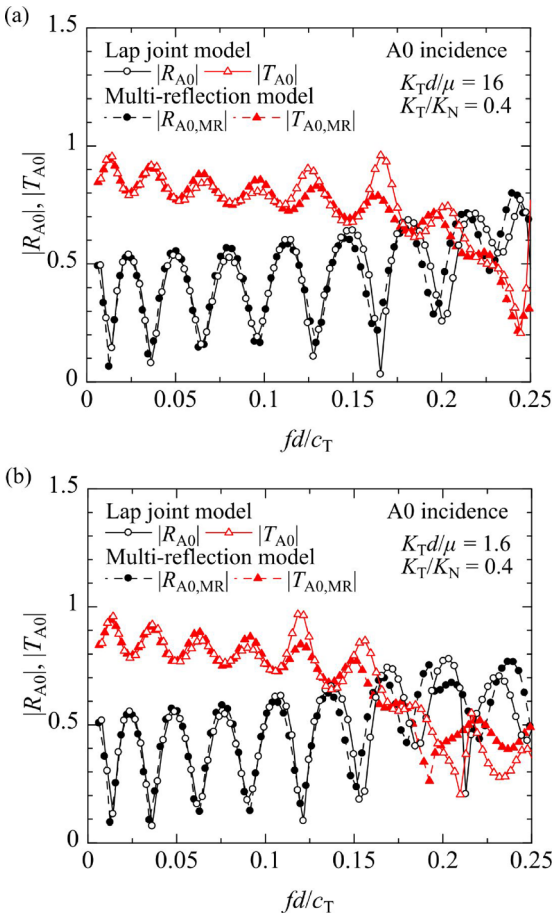

FIG. 8. (Color online) Comparison of the A0 mode reflection and transmission coefficients for the A0 mode incidence obtained from the multi-reflection model to the results for the lap joint model. The tangential stiffness is set as (a) $K_T d/\mu = 16$ and (b) $K_T d/\mu = 1.6$ at a stiffness ratio $K_T/K_N = 0.4$.

Likewise, it is shown by the multi-reflection model that the local maxima and minima of the S0 mode reflection and transmission coefficients for the A0 mode incidence shown in Figs. 3(c) and 3(d) can be attributed to the wave interference by the DS0 mode as well as the DA0 mode. However, detailed data are not shown here. The reflection and transmission coefficients of the S0 mode have local maximum and minimum frequencies depending on the coupling effect of the DS0 and DA0 modes.

To clarify the reason for which the DA0 mode plays an essential role in the reflection and transmission coefficients of the A0 mode for the A0 mode incidence, the mode profiles of the guided waves are examined. The displacement distributions of the S0 and A0 modes in the lower adherend, i.e., a single-layer plate of thickness d, are shown along the thickness (z) direction in Figs. 9(a) and 9(b), respectively, at a normalized frequency of $fd/c_T = 0.15$. The in-plane displacement u_x and the out-of-plane displacement u_z are normalized by their maximum value in each figure. At the same frequency f, the displacement profiles of the DS0 and DA0 modes in the overlap region, i.e., a double-layer plate of thickness $2d$, are shown in Figs. 9(c) and 9(d) for $K_T d/\mu = 16$ and $K_T/K_N = 0.4$, respectively. The profiles of the DS0 and DA0 modes at $K_T d/\mu = 1.6$ and $K_T/K_N = 0.4$ are also shown in Figs. 9(e) and 9(f), respectively. The displacement components are normalized similarly to Figs. 9(a) and 9(b) in Figs. 9(c)–9(f). The out-of-displacement u_z of the DA0 mode is large compared to the in-plane displacement u_x, while the in-plane displacement component is dominant in the profile of the DS0 mode. Basically, when the A0 mode is incident from the lower adherend $-d < z < 0$ to a joint edge, guided wave modes whose profiles in $-d < z < 0$ are close to the incident A0 mode are expected to mainly generate in the overlap region.[12,14,17,18] The region of $-d < z < 0$ is filled with gray color in Figs. 9(a)–9(f) for comparison. In Figs. 9(a)–9(f), the DA0 mode shows a closer profile to the A0 mode in $-d < z < 0$ than the DS0 mode, which indicates that the DA0 mode is mainly transmitted in the overlap region for the A0 mode incidence. Likewise, for the DA0 mode incidence from the overlap region to a joint edge, the A0 mode is mainly transmitted in a single plate region due to the similarity of the mode profiles.

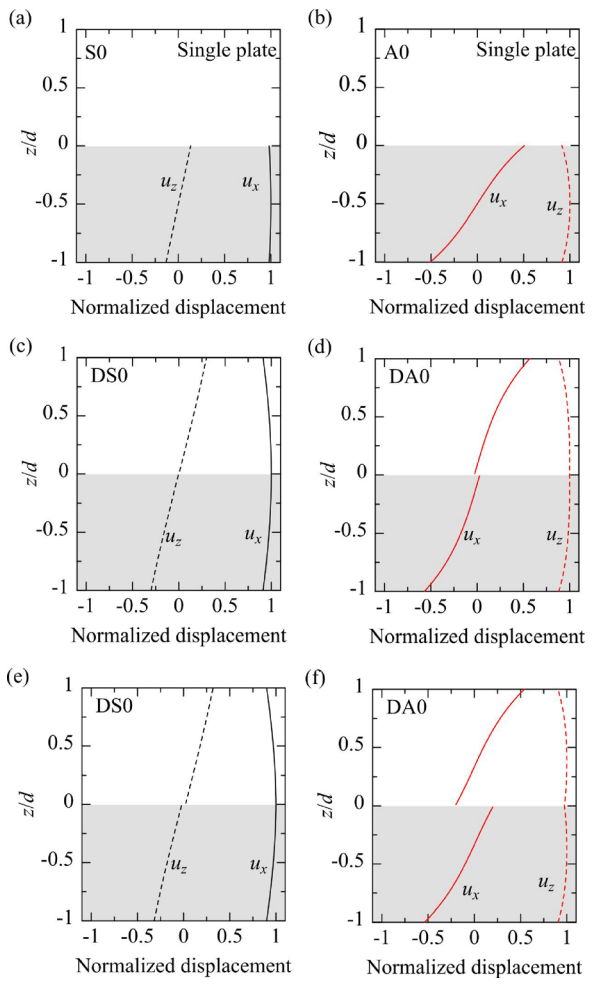

FIG. 9. (Color online) Displacement profiles of the (a) S0 and (b) A0 modes at a normalized frequency of $fd/c_T = 0.15$ in a single-layer plate of thickness d, the (c) DS0 and (d) DA0 modes at the same frequency f in a double-layer plate for $K_T d/\mu = 16$, and the (e) DS0 and (f) DA0 modes for $K_T d/\mu = 1.6$ at a stiffness ratio $K_T/K_N = 0.4$.

Since the mode profile of the A0 mode and that of the DA0 mode in an adherend are not perfectly identical, mode conversion between antisymmetric and symmetric modes at a joint edge occurs to some extent. This fact corresponds to the non-negligible values of the S0 mode reflection and transmission coefficients in Figs. 3(c) and 3(d). However, as described above, the effect of the DS0 mode on the A0 mode reflection and transmission coefficients across the entire joint is not significant. This feature appears because the reflected (or transmitted) A0 mode components derived from the DS0 mode have undergone the mode conversion between the antisymmetric and symmetric modes at the joint edges more than twice. The wave components that have undergone the mode conversion multiple times seem to become negligible.

C. Peak frequencies of the A0 mode transmission coefficient

It has been shown in Secs. III A and III B that the A0 mode reflection and transmission coefficients for the A0 mode incidence exhibit local maxima and minima at multiple frequencies. In this section, the peak frequencies f_p at which the transmission coefficient of the A0 mode shows local maxima are further investigated. The amplitude transmission coefficients of the A0 mode are calculated for different joint conditions, and their normalized peak frequencies $F_p = f_p d/c_T$ are extracted as functions of the tangential stiffness and the stiffness ratio.

The normalized peak frequencies F_p at a stiffness ratio $K_T/K_N = 0.4$ are shown as functions of the normalized tangential stiffness in Fig. 10(a). Dashed lines represent the peak frequencies for infinite normal and tangential stiffnesses, at which the continuity condition is applied to the displacement and stress components at the joint. Nine peak frequencies, which are located in $fd/c_T < 0.3$ at infinite stiffnesses, are traced with the tangential stiffness decreased in Fig. 10(a). From Fig. 10(a), the normalized peak frequencies below 0.05 are shown to be almost invariant in $K_T d/\mu > 0.1$, but in a higher frequency range the peak frequencies decrease with decreasing tangential stiffness. This feature appears because the dispersion relation of the DA0 mode, which is closely associated with the local maxima of the A0 mode transmission coefficient, does not greatly depend on the tangential stiffness in $fd/c_T < 0.05$ as shown in Fig. 7(b). The peak frequencies located in a sufficiently low frequency range are determined mainly by the length of the overlap joint L.

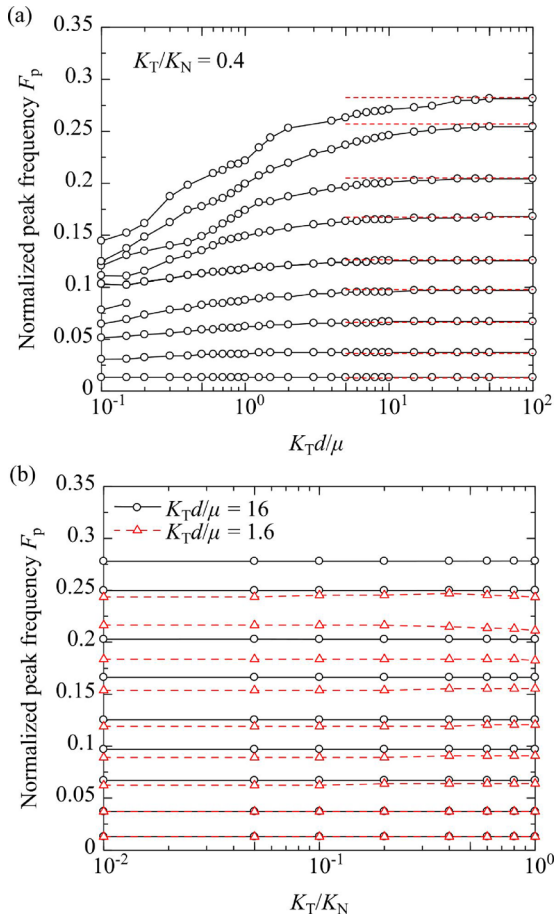

FIG. 10. (Color online) Relations of the normalized peak frequencies of the A0 mode transmission coefficient for the A0 mode incidence to (a) the normalized tangential stiffness $K_T d/\mu$ at a stiffness ratio $K_T/K_N = 0.4$ and (b) the stiffness ratio at two fixed tangential stiffnesses. Dashed lines in (a) represent the peak frequencies at infinite stiffnesses.

Furthermore, the effect of the stiffness ratio K_T/K_N on the peak frequencies is investigated. The normalized peak frequencies at two fixed tangential stiffnesses $K_T d/\mu = 16$ and $K_T d/\mu = 1.6$ are shown as functions of K_T/K_N in Fig. 10(b). The obtained results show that the peak frequencies depend on the tangential stiffness but not significantly on the stiffness ratio. In other words, the peak frequencies are found to be nominally invariant with the normal stiffness of the lap joint. The results in Figs. 10(a) and 10(b) imply that the estimation of the tangential stiffness could be possible from the peak frequencies of the A0 mode transmission coefficient for the A0 mode incidence. The selective dependence of the peak frequencies on the tangential stiffness can be attributed to the interference of waves originating from the multiple reflection of the DA0 mode between the joint edges, which has been described in Sec. III B. Since the dispersion relation of the DA0 mode is determined by the tangential stiffness, the peak frequencies of the A0 mode transmission coefficient are considered to be insensitive to the normal stiffness. The procedure to identify the peak frequencies from temporal waveforms is further examined by time-domain numerical simulation in Sec. IV.

In Figs. 4(c) and 4(d), the reflection and transmission coefficients of the S0 mode also show local maximum and minimum frequencies, which are invariant with the normal stiffness, analogously to the A0 mode coefficients in Figs. 4(a) and 4(b). As described briefly in Sec. III B, the local maxima and minima of the S0 mode reflection and transmission coefficients occur due to the wave interference by not only the DA0 mode but also the DS0 mode, whose dispersion relation basically depends on the normal stiffness. However, as shown in Fig. 7(a), the dispersion relation of the DS0 mode is not significantly affected by the normal stiffness in a low frequency range of $fd/c_T < 0.25$. Thus the peak frequencies of the S0 mode coefficients are nominally independent of the normal stiffness in the low frequency range. These peak frequencies could also be useful for the estimation of the tangential stiffness, but this topic is not further considered in the present paper.

IV. TIME-DOMAIN NUMERICAL SIMULATION

A. Numerical model

In this section, the procedure to identify the local maximum and minimum frequencies of the reflection and transmission coefficients is investigated by using temporal waveforms based on the time-domain numerical simulation. The reflection and transmission measurements for the A0 mode incidence are simulated using the time-domain FEM. The numerical model for the time-domain analysis is schematically shown in Fig. 11. In the Cartesian x-z coordinate system, two isotropic elastic plates with the material property given in Sec. II A are overlapped in $|x| < L/2$ under the plane-strain condition. The thickness of the adherends is $d = 2$ mm, and the joint length is $L = 15d = 30$ mm. The spring-type interface condition is applied at $z = 0$ in the overlap region $|x| < L/2$. To excite the A0 mode in the lower adherend, the out-of-plane stress component σ_z is antisymmetrically applied on two surface areas P_1 and P_2,[39,40] whose width is 5 mm. Namely, when an input waveform $g(t)$ is prescribed as the out-of-plane stress component uniformly in the area P_1, the out-of-plane stress in P_2 is given as $-g(t)$. In this study, a Gaussian-modulated tone-burst expressed as

$$g(t) = \exp\left[-\left(\frac{t - t_0}{\sigma_0}\right)^2\right]\sin[2\pi f_0(t - t_0)] \tag{7}$$

was used as the input waveform, where $f_0 = 0.25$ MHz, $t_0 = 20\,\mu$s, and $\sigma_0 = 2\,\mu$s. The center frequency of the input waveform f_0 corresponds to the normalized frequency $f_0 d/c_T = 0.16$, at which only the S0 and A0 modes can propagate in the adherends. The horizontal distance between the left joint

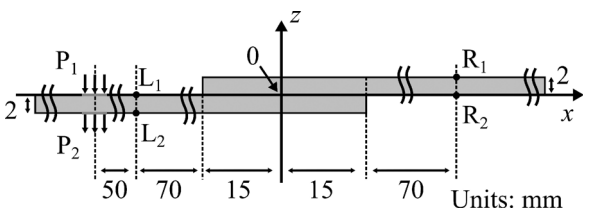

FIG. 11. Numerical model of a single lap joint for the time-domain analysis.

edge and the center location of the areas P_1 and P_2 is 120 mm.

The waveforms of the excited Lamb waves were calculated at four points, L_1 and L_2 on the surfaces of the lower adherend, and R_1 and R_2 on the upper adherend. The points L_1 and L_2 are symmetrically located at $x = -85$ mm with respect to the middle plane of the lower adherend, and their horizontal distance to the left edge of the joint is 70 mm. By adding the out-of-plane displacements calculated at L_1 and L_2, the waveform of the S0 mode is canceled and the waveforms of the incident and reflected A0 modes are selectively obtained due to the symmetry of the mode profiles. Similarly, the points R_1 and R_2 are symmetrically located on the surfaces of the upper adherend at $x = 85$ mm, and the waveform of the transmitted A0 mode is selectively obtained from the waveforms calculated at R_1 and R_2. Their horizontal distance to the right joint edge is 70 mm. To eliminate the effect of the reflection at the free edges of the adherends, the length of the adherends was set as a sufficiently large value, 400 mm.

The time-domain finite element simulation was carried out to analyze the Lamb wave interaction with the lap joint. The numerical model of Fig. 11 was discretized by four-node square-shaped isoparametric elements, which had the same dimensions as used in the analysis by HFEM. A lumped mass matrix approximation was applied, and the time integration was performed in an explicit scheme using the fourth-order Runge-Kutta method. The time increment was set as 0.02 μs to satisfy the stability condition.

B. Numerical simulation results

The numerical simulation was carried out for two different tangential stiffnesses $K_T d/\mu = 16$ and $K_T d/\mu = 1.6$, i.e., $K_T \approx 0.2$ GPa/μm and $K_T \approx 0.02$ GPa/μm, at a stiffness ratio $K_T/K_N = 0.4$. The waveforms of the A0 mode calculated at $x = -85$ mm and $x = 85$ mm are shown in Figs. 12(a) and 12(b), respectively. In Fig. 12(a), the incident A0 mode is located at around 38 μs, and then the A0 mode reflected from the lap joint arrives after 75 μs. The reflected A0 mode has a few wave packets due to the multiple reflection in the overlap region. The first reflected wave packet is located at around 85 μs for both $K_T d/\mu = 16$ and $K_T d/\mu = 1.6$, but the second wave packet for $K_T d/\mu = 16$ arrives at around 104 μs, which is slightly earlier than the one for $K_T d/\mu = 1.6$ (106 μs). The waveforms of the transmitted A0 mode are shown in Fig. 12(b) as well. The transmission waveforms show long-oscillation tails until around 140 μs, whose shapes are different for $K_T d/\mu = 16$ and $K_T d/\mu = 1.6$. The time length of the transmission waveforms is approximately 55 μs, which is longer than the length of the incident waveform in Fig. 12(a), 20 μs.

The incident A0 mode is extracted from the waveforms in Fig. 12(a) by a smooth rectangular gate function in $10\ \mu\text{s} < t < 50\ \mu\text{s}$, and its amplitude spectrum is calculated by spectral analysis using fast Fourier transform (FFT). Analogously, the amplitude spectra of the reflected and transmitted A0 modes are calculated using a smooth rectangular gate of $60\ \mu\text{s} < t < 170\ \mu\text{s}$, which is called gate 1 in this section. The ratio of the reflected wave amplitude spectrum to the incident wave spectrum is obtained as the reflection

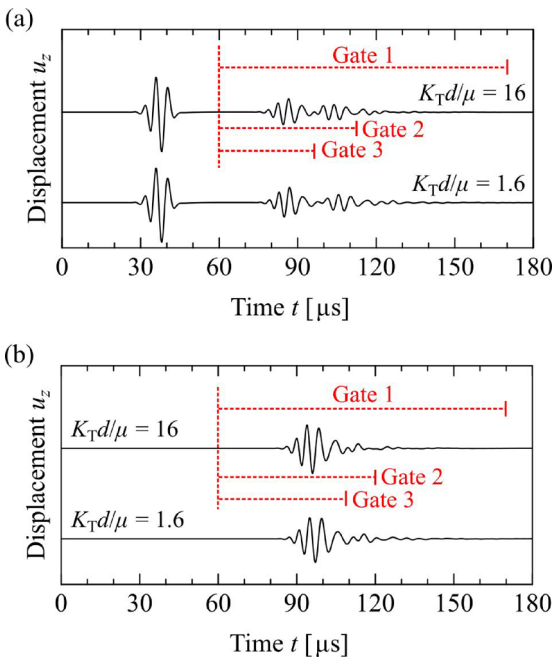

FIG. 12. (Color online) Time histories of (a) the incident and reflected A0 modes calculated from the waveforms at L_1 and L_2, and (b) the transmitted A0 mode calculated from the waveforms at R_1 and R_2. Time gates for the spectral analysis are shown together.

coefficient, and likewise the transmission coefficient is calculated from the amplitude spectra. The obtained reflection and transmission coefficients are shown in Figs. 13(a) and 13(b) as functions of frequency f, and are compared to the results by the frequency-domain analysis using the HFEM. The incidence of the A0 mode at a single frequency has been considered in the frequency-domain analysis by the HFEM, while the transient behavior for the pulse wave incidence is examined here by time-domain FEM. The results by time-domain FEM show slight deviation in a relatively high frequency range, but both results are in good agreement in the vicinity of the center frequency of the input waveform (0.25 MHz). In particular, the local maxima and minima of the A0 mode reflection and transmission coefficients are well reproduced by the time-domain numerical simulation. This agreement results from the sufficiently long gate function for the spectral analysis of the reflection and transmission waveforms.

The reflection and transmission coefficients calculated from the temporal waveforms depend on the time range of the gate functions in the spectral analysis. The effect of the gate range on the reflection coefficient at $K_T d/\mu = 16$ and $K_T/K_N = 0.4$ is shown in Fig. 14(a) for three different gates, gates 1–3, which are indicated in Fig. 12(a). In Fig. 12(a), gate 1 includes the entire waveform of the reflected A0 mode and corresponds to the reflection coefficient shown in Fig. 13(a), while gates 2 ($60\ \mu\text{s} < t < 113\ \mu\text{s}$) and 3 ($60\ \mu\text{s} < t < 96\ \mu\text{s}$) extract parts of the reflection waveform. Since two wave packets are located in the time range of gate 2, the reflection coefficient calculated by gate 2 shows local maxima and minima in Fig. 14(a). However, in the case of gate 3, which includes only the first wave packet of the reflected wave, the reflection coefficient varies almost monotonically below 0.3 MHz, and its peak behavior is not observed in the low

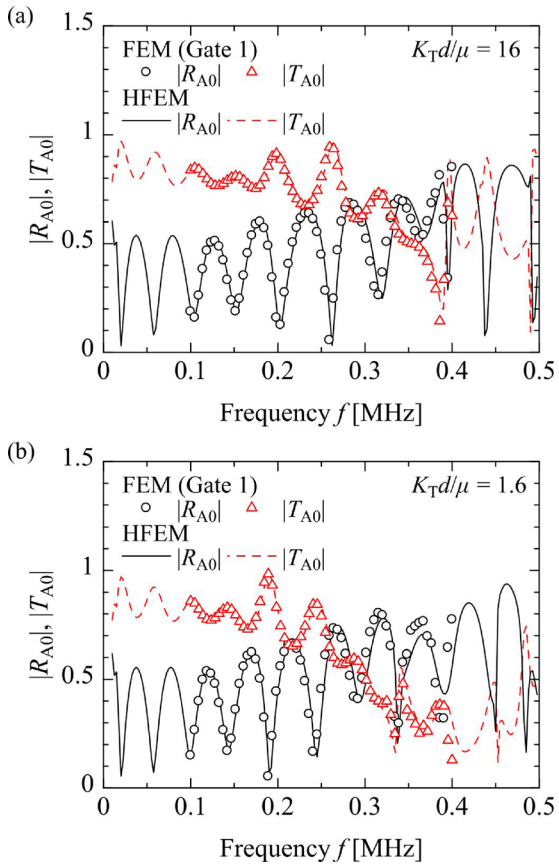

FIG. 13. (Color online) Comparison of the A0 mode reflection and transmission coefficients for the A0 mode incidence calculated by FEM to the results by HFEM, for (a) $K_T d/\mu = 16$ and (b) $K_T d/\mu = 1.6$ at a stiffness ratio $K_T/K_N = 0.4$. Gate 1 was used in the spectral analysis for the results by FEM.

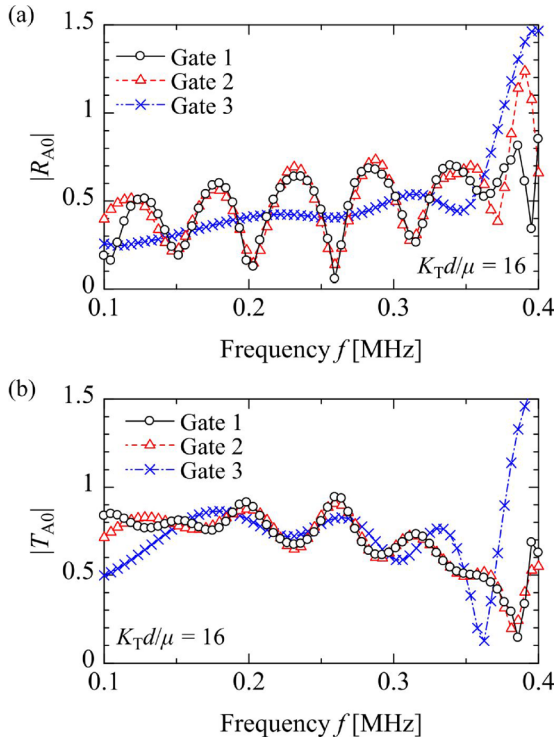

FIG. 14. (Color online) Effect of the time gate range on the (a) reflection and (b) transmission coefficients of the A0 mode for the A0 mode incidence. The tangential stiffness and the stiffness ratio are set as $K_T d/\mu = 16$ and $K_T/K_N = 0.4$, respectively.

frequency range. This result indicates that the tail part of the reflection waveform is necessary to identify the local maxima and minima of the reflection coefficient.

A similar investigation is performed for the transmission coefficient of the A0 mode. The effect of the gate range on the transmission coefficient is shown in Fig. 14(b) for three different gates, gates 1–3, which are indicated in Fig. 12(b). Gate 1 ($60\,\mu s < t < 170\,\mu s$) includes the entire waveform of the transmitted A0 mode and corresponds to the transmission coefficient in Fig. 13(a), while gates 2 ($60\,\mu s < t < 120\,\mu s$) and 3 ($60\,\mu s < t < 109\,\mu s$) extract parts of the transmission waveform. In Fig. 14(b), the result for gate 2 fairly reproduces the local maxima and minima of the transmission coefficient calculated by gate 1 above 0.18 MHz. However, the result for gate 3, which has a relatively short time range compared to gate 2, deviates from the results by gates 1 and 2 in the entire frequency range. In particular, the peak frequencies are not precisely identified if gate 3 is used in the spectral analysis. Analogously to the reflection coefficient, the tail part of the transmission waveform is necessary to precisely obtain the local maximum and minimum frequencies of the A0 mode transmission coefficient.

V. CONCLUSIONS

In this study, the reflection and transmission characteristics of Lamb waves at an adhesively bonded single lap joint have been theoretically investigated. The adhesive joint has been modeled as a linear spring-type interface, which is characterized by normal and tangential stiffnesses, and the HFEM has been employed for the theoretical analysis. For the incidence of the lowest-order antisymmetric (A0) mode, it has been shown that the reflection and transmission coefficients of the A0 mode vary with frequency and tangential stiffness in complicated manners. In particular, the reflection and transmission coefficients of the A0 mode have shown local maxima and minima at multiple frequencies due to the wave interference originating from the antisymmetric guided wave mode in the overlap region. Furthermore, the peak frequencies of the A0 mode transmission coefficient have been shown to depend on the tangential stiffness, not significantly on the normal stiffness. This feature indicates that the tangential stiffness could be estimated from the peak frequencies of the A0 mode transmission coefficient. To discuss the procedure to identify the local maximum and minimum frequencies of the reflection and transmission coefficients, a time-domain numerical simulation has been carried out by FEM. As a result, it has been found that the local maximum and minimum frequencies of the A0 mode reflection and transmission coefficients can be obtained from the temporal waveforms if time gates for the spectral analysis are sufficiently wide to include the tails of the reflection and transmission waveforms.

ACKNOWLEDGMENTS

This study has been supported by Grants-in-Aid for Scientific Research (KAKENHI) Grant Nos. JP17H07254 and JP18K13663 from the Japan Society for the Promotion of Science (JSPS). The authors thank the anonymous reviewers for providing constructive and insightful comments.

[1]C. C. Guyott, P. Cawley, and R. D. Adams, "The non-destructive testing of adhesively bonded structure: A review," J. Adhes. **20**, 129–159 (1986).
[2]R. D. Adams and P. Cawley, "A review of defect types and nondestructive testing techniques for composites and bonded joints," NDT Int. **21**, 208–222 (1988).
[3]P. N. Dewen and P. Cawley, "Ultrasonic determination of the cohesive properties of bonded joints by measurement of reflection coefficient and bondline transit time," J. Adhes. **40**, 207–227 (1993).
[4]A. Pilarski and J. L. Rose, "A transverse-wave ultrasonic oblique-incidence technique for interfacial weakness detection in adhesive bonds," J. Appl. Phys. **63**, 300–307 (1988).
[5]P. B. Nagy, "Ultrasonic detection of kissing bonds at adhesive interfaces," J. Adhes. Sci. Technol. **5**, 619–630 (1991).
[6]W. Wang and S. I. Rokhlin, "Evaluation of interfacial properties in adhesive joints of aluminum alloys using angle-beam ultrasonic spectroscopy," J. Adhes. Sci. Technol. **5**, 647–666 (1991).
[7]A. Pilarski and J. L. Rose, "Lamb wave mode selection concepts for interfacial weakness analysis," J. Nondestruct. Eval. **11**, 237–249 (1992).
[8]T. Kundu and K. Maslov, "Material interface inspection by Lamb waves," Int. J. Solids Struct. **34**, 3885–3901 (1997).
[9]J. L. Rose, *Ultrasonic Waves in Solid Media* (Cambridge University Press, Cambridge, 1999), Chap. 8, 15.
[10]S. I. Rokhlin, "Lamb wave interaction with lap-shear adhesive joints: Theory and experiment," J. Acoust. Soc. Am. **89**, 2758–2765 (1991).
[11]K. Heller, L. J. Jacobs, and J. Qu, "Characterization of adhesive bond properties using Lamb waves," NDT&E Int. **33**, 555–563 (2000).
[12]M. J. S. Lowe, R. E. Challis, and C. W. Chan, "The transmission of Lamb waves across adhesively bonded lap joints," J. Acoust. Soc. Am. **107**, 1333–1345 (2000).
[13]R. Seifried, L. J. Jacobs, and J. Qu, "Propagation of guided waves in adhesive bonded components," NDT&E Int. **35**, 317–328 (2002).
[14]F. Lanza di Scalea, P. Rizzo, and A. Marzani, "Propagation of ultrasonic guided waves in lap-shear adhesive joints: Case of incident a0 Lamb wave," J. Acoust. Soc. Am. **115**, 146–156 (2004).
[15]Y. Okabe, J. Kuwahara, K. Natori, N. Takeda, T. Ogisu, S. Kojima, and S. Komatsuzaki, "Evaluation of debonding progress in composite bonded structures using ultrasonic waves received in fiber Bragg grating sensors," Smart Mater. Struct. **16**, 1370–1378 (2007).
[16]B. Le Crom and M. Castaings, "Shear horizontal guided wave modes to infer the shear stiffness of adhesive bond layers," J. Acoust. Soc. Am. **127**, 2220–2230 (2010).
[17]B. Ren and C. J. Lissenden, "Ultrasonic guided wave inspection of adhesive bonds between composite laminates," Int. J. Adhes. Adhes. **45**, 59–68 (2013).
[18]P. Puthillath, J. M. Galan, B. Ren, C. J. Lissenden, and J. L. Rose, "Ultrasonic guided wave propagation across waveguide transitions: Energy transfer and mode conversion," J. Acoust. Soc. Am. **133**, 2624–2633 (2013).
[19]M. Castaings, "SH ultrasonic guided waves for the evaluation of interfacial adhesion," Ultrasonics **54**, 1760–1775 (2014).
[20]E. Siryabe, M. Renier, A. Meziane, and M. Castaings, "The transmission of Lamb waves across adhesively bonded lap joints to evaluate interfacial adhesive properties," Phys. Procedia. **70**, 541–544 (2015).
[21]N. Mori and S. Biwa, "Transmission of Lamb waves and resonance at an adhesive butt joint of plates," Ultrasonics **72**, 80–88 (2016).
[22]C. Gauthier, M. Ech-Cherif El-Kettani, J. Galy, M. Predoi, D. Leduc, and J. L. Izbicki, "Lamb waves characterization of adhesion levels in aluminum/epoxy bi-layers with different cohesive and adhesive properties," Int. J. Adhes. Adhes. **74**, 15–20 (2017).
[23]R. Alebrahim, "Peridynamic modeling of Lamb wave propagation in bimaterial plates," Compos. Struct. **214**, 12–22 (2019).
[24]H. G. Tattersall, "The ultrasonic pulse-echo technique as applied to adhesion testing," J. Phys. D. Appl. Phys. **6**, 819–832 (1973).
[25]M. Schoenberg, "Elastic wave behavior across linear slip interfaces," J. Acoust. Soc. Am. **68**, 1516–1521 (1980).
[26]J. M. Baik and R. B. Thompson, "Ultrasonic scattering from imperfect interfaces: A quasi-static model," J. Nondestruct. Eval. **4**, 177–196 (1984).
[27]S. I. Rokhlin and Y. J. Wang, "Analysis of boundary conditions for elastic wave interaction with an interface between two solids," J. Acoust. Soc. Am. **89**, 503–515 (1991).
[28]B. Hosten and M. Castaings, "Finite elements methods for modeling the guided waves propagation in structures with weak interfaces," J. Acoust. Soc. Am. **117**, 1108–1113 (2005).
[29]P. Fraisse, F. Schmit, and A. Zarembowitch, "Ultrasonic inspection of very thin adhesive layers," J. Appl. Phys. **72**, 3264–3271 (1992).
[30]Z. Fan, M. Castaings, M. J. S. Lowe, C. Biateau, and P. Fromme, "Feature-guided waves for monitoring adhesive shear modulus in bonded stiffeners," NDT&E Int. **54**, 96–102 (2013).
[31]M. Koshiba, S. Karakida, and M. Suzuki, "Finite-element analysis of Lamb wave scattering in an elastic plate waveguide," IEEE Trans. Sonics Ultrason. **31**, 18–24 (1984).
[32]A. Mal and Z. Chang, "A semi-numerical method for elastic wave scattering calculations," Geophys. J. Int. **143**, 328–334 (2000).
[33]N. Terrien, D. Osmont, D. Royer, F. Lepoutre, and A. Déom, "A combined finite element and modal decomposition method to study the interaction of Lamb modes with micro-defects," Ultrasonics **46**, 74–88 (2007).
[34]N. Mori, S. Biwa, and T. Hayashi, "Reflection and transmission of Lamb waves at an imperfect joint of plates," J. Appl. Phys. **113**, 074901 (2013).
[35]W. Song, J. L. Rose, J. M. Galán, and R. Abascal, "Ultrasonic guided wave scattering in a plate overlap," IEEE Trans. Ultrason. Ferroelectr. Freq. Control **52**, 892–903 (2005).
[36]S. Mezil, J. Laurent, D. Royer, and C. Prada, "Non contact probing of interfacial stiffnesses between two plates by zero-group velocity Lamb modes," Appl. Phys. Lett. **105**, 021605 (2014).
[37]L. M. Brekhovskikh, *Waves in Layered Media*, 2nd ed. (Academic, New York, 1976), pp. 15–23.
[38]A. I. Lavrentyev and S. I. Rokhlin, "Ultrasonic spectroscopy of imperfect contact interfaces between a layer and two solids," J. Acoust. Soc. Am. **103**, 657–664 (1998).
[39]C. Yang, L. Ye, Z. Su, and M. Bannister, "Some aspects of numerical simulation for Lamb wave propagation in composite laminates," Compos. Struct. **75**, 267–275 (2006).
[40]N. Mori, S. Biwa, and T. Kusaka, "Damage localization method for plates based on the time reversal of the mode-converted Lamb waves," Ultrasonics **91**, 19–29 (2019).